Visual control of flight speed in *Drosophila melanogaster*

Steven N. Fry[1,2,*], Nicola Rohrseitz[1], Andrew D. Straw[3] and Michael H. Dickinson[3]

[1]Institute of Neuroinformatics, University of Zürich and ETH Zürich, Switzerland, [2]Institute of Robotics and Intelligent Systems, ETH Zürich, Switzerland and [3]Bioengineering, California Institute of Technology, MC 138-78, Pasadena, CA 91125, USA
*Author for correspondence (e-mail: steven@ini.ch)

SUMMARY

Flight control in insects depends on self-induced image motion (optic flow), which the visual system must process to generate appropriate corrective steering maneuvers. Classic experiments in tethered insects applied rigorous system identification techniques for the analysis of turning reactions in the presence of rotating pattern stimuli delivered in open-loop. However, the functional relevance of these measurements for visual free-flight control remains equivocal due to the largely unknown effects of the highly constrained experimental conditions. To perform a systems analysis of the visual flight speed response under free-flight conditions, we implemented a 'one-parameter open-loop' paradigm using 'TrackFly' in a wind tunnel equipped with real-time tracking and virtual reality display technology. Upwind flying flies were stimulated with sine gratings of varying temporal and spatial frequencies, and the resulting speed responses were measured from the resulting flight speed reactions. To control flight speed, the visual system of the fruit fly extracts linear pattern velocity robustly over a broad range of spatio–temporal frequencies. The speed signal is used for a proportional control of flight speed within locomotor limits. The extraction of pattern velocity over a broad spatio–temporal frequency range may require more sophisticated motion processing mechanisms than those identified in flies so far. In *Drosophila*, the neuromotor pathways underlying flight speed control may be suitably explored by applying advanced genetic techniques, for which our data can serve as a baseline. Finally, the high-level control principles identified in the fly can be meaningfully transferred into a robotic context, such as for the robust and efficient control of autonomous flying micro air vehicles.

Supplementary material available online at http://jeb.biologists.org/cgi/content/full/212/8/1120/DC1

Key words: *Drosophila*, flight control, behavior, vision.

INTRODUCTION

Flying insects exhibit impressive flight control capabilities that far outperform human technology. The challenge of controlling stable flapping flight in these small animals is met with highly specialized reflexive sensorimotor pathways that need to operate at short time spans. Self-induced image motion, or optic flow (Gibson, 1958), provides insects with an external frame of reference [allocentric cues (Wehner, 1992)], which plays a particularly important role in the control of various aspects of flight, such as altitude and flight speed (for a review, see Collett et al., 1993). Therefore, the mechanisms underlying the processing of optic flow by the visual system and the means by which it can generate appropriate motor control signals for velocity and course control have been met with strong research interest over the past several decades (for reviews, see Egelhaaf and Kern, 2002; Srinivasan and Zhang, 2004) [for a recent paper on visual free-flight control in *Drosophila*, see Mronz and Lehmann (Mronz and Lehmann, 2008)].

Rotational control

Classic studies of visual motion processing (Hassenstein and Reichardt, 1956; Kunze, 1961; Fermi and Reichardt, 1963; Götz, 1964; Eckert, 1973) applied a black-box approach in which the visual processing mechanisms were inferred from the turning responses measured from tethered walking or flying insects in the presence of rotating gratings of varying temporal and spatial frequencies (Fig. 1A). Because tethering breaks the reafferent visual coupling normally experienced during free movements, this preparation allows arbitrary visual stimuli to be presented to an insect without

the animal's behavioral response affecting the sensory input in any way [open-loop condition (e.g. Taylor et al., 2008)].

A characteristic feature of optomotor turning responses to visual gratings is their tuning to a particular angular spatial frequency [*sf* (the number of cycles per unit visual arc)] and a particular temporal frequency [*tf* (the number of cycles passing a given point on the retina per unit time)] (reviewed by Buchner, 1984; Srinivasan et al., 1999). This observation, first made by Hassenstein and Reichardt in walking *Chlorophanus* beetles (Hassenstein and Reichardt, 1956), has been repeatedly confirmed in tethered preparations using walking [e.g. *Drosophila* (Buchner, 1976)] and flying [Apis (Kunze, 1961); *Drosophila* (Götz, 1964)] insects. The spatio–temporal response properties are consistent with the predictions of the influential 'correlation-type' motion detector model (Fig. 1B), proposed by Reichardt (Reichardt, 1961) almost 50 years ago. According to this model, motion signals are computed locally by elementary motion detectors (EMDs) from a spatio–temporal correlation of intensity signals sensed in neighboring visual channels (for reviews, see Buchner, 1984; Borst and Egelhaaf, 1989; Egelhaaf and Borst, 1993; Hausen, 1993; Borst and Haag, 2002). This view is consistent with a broad body of electrophysiological evidence showing that inputs of correlation-type EMDs are integrated by the well-characterized lobula plate tangential cells (LPTC), whose outputs are believed to represent control signals for corrective steering maneuvers (for reviews, see Egelhaaf and Borst, 1993; Borst and Haag, 2002).

Translational flight control

Visual behaviors have also been explored extensively in freely flying insects (Collett et al., 1993; Srinivasan and Zhang, 2004). Most of the available data have been obtained from honeybees, which can be easily trained to fly through experimental setups under well-controlled conditions. In various experiments and behavioral contexts, honeybees have been shown to maintain a consistent flight speed with respect to a perceived pattern, irrespective of its spatial frequency and contrast (Srinivasan et al., 1991; Srinivasan et al., 1996; Baird et al., 2005).

This phenomenon, often referred to as 'pattern invariance' or 'velocity dependence', is not limited to honeybees. Similar evidence has emerged from free-flight studies performed in other insects, including fruit flies. David (David, 1982), for example, induced *Drosophila virilis* to hover stationary in a wind tunnel by manually adjusting the speed of a surrounding 'barber's pole' pattern. He showed that the flies hovered at a particular 'preferred' pattern speed, irrespective of whether the pattern consisted of broad (72 deg.) or narrow (40 deg.) stripes [see fig. 8 in David (David, 1982)]. Furthermore, he showed that the preferred flight speed was invariant to substantial changes in headwind [see fig. 3 in David (David, 1982)], as is the case in other insect species [e.g. *Aedes* (Kennedy, 1939); *Apis* (Barron and Srinivasan, 2006)]. The strict dependence on optic flow makes flight speed control a powerful model behavior to characterize optic flow processing in the context of free flight.

Does a common visual pathway underlie rotational and translational responses?

The observed pattern-invariant flight responses of flies stand in apparent contradiction to the spatio–temporal tuning properties of optomotor turning responses and the motion-processing pathways of flies [e.g. the LPTCs in *Drosophila* (Joesch et al., 2008)]. Various suggestions have been put forth to explain pattern-invariant behaviors based on the known mechanisms of motion computation, including hypothetical correlation-based mechanisms (Zanker et al., 1999), or higher order motion processing circuits that extract a more accurate velocity estimate from arrays of differently tuned correlators (Srinivasan et al., 1999). More recently, the sensory and behavioral ecology of visual flight control have received increased attention. This more ethological approach suggests that the known properties of motion-sensitive visual interneurons will make more functional sense if the spatio–temporal properties of real visual scenes are taken into account, including an insect's actual body motion during flight maneuvers (O'Carroll et al., 1996; Egelhaaf et al., 1998; Egelhaaf et al., 2002; Lindemann et al., 2005; Straw et al., 2008). The relevance of experiments performed using highly controlled but partially unrealistic laboratory conditions deserves explicit attention.

The apparent discrepancy in the motion processing mechanisms observed from turning and flight speed responses may relate to the disparate conditions under which the experiments were performed. First, turning responses were measured in the presence of panoramic patterns of constant angular wavelength whereas flight speed responses were measured using planar patterns (compare Fig. 1A with Fig. 1C; also see Fig. 2B). From the vantage point of the fly, the planar pattern is geometrically distorted such that the angular wavelength (λ) of the pattern is maximal at lateral positions and decreases toward frontal and caudal positions (Fig. 2B). Second, turning responses were measured under tethered conditions, in which various sensory feedback loops relevant for flight control are broken (Taylor et al., 2008). The interruption of feedback loops, in particular haltere feedback, is the likely cause for significant behavioral artifacts
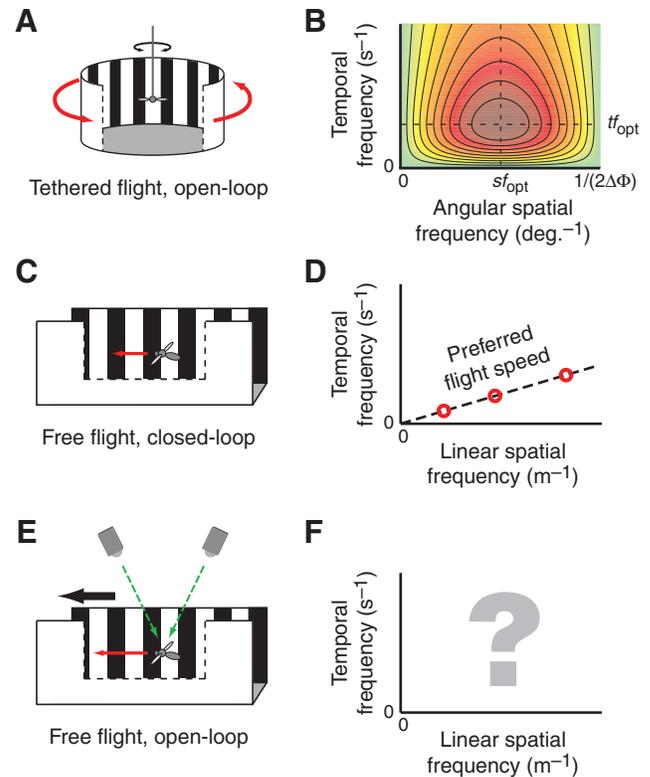

Fig. 1. Experimental analysis of optomotor turning and visual flight speed responses. (A) Optomotor turning response paradigm. An insect is tethered within a patterned rotating drum and its steady-state turning responses are measured. Because the body is fixed, the behavioral reactions have no effect on the perceived stimulus (open-loop condition). (B) Idealized spatio–temporal tuning of optomotor turning reactions. The response surface represents the steady-state output of a basic correlation-type motion detector scheme, calculated using the equations applicable for sine grating stimuli provided by Borst and Bahde (Borst and Bahde, 1986). Normalized response strength (green and dark red correspond to values between 0 and 1, respectively) is plotted as a function of the temporal frequency (tf, in s^{-1}) and angular spatial frequency (sf, in deg.$^{-1}$) of sine grating patterns. Optomotor turning responses are maximally elicited by a particular optimal temporal frequency (tf_{opt}) and optimal spatial frequency (sf_{opt}). (C) Standard flight speed paradigm. An insect is induced to fly along a patterned channel and its flight speed is measured under steady-state conditions. The insect adjusts its flight speed according to the perceived visual feedback from the pattern (closed-loop condition). (D) Flight speed measurements in the presence of sine grating patterns with varying linear spatial frequency (SF, in m^{-1}). Insects adjust their flight speed as to hold constant the ratio of temporal and linear spatial frequency, such that measurements (red circles) fall on a diagonal line in the TF–SF parameter space, which corresponds to the insect's preferred velocity ($V_{pref}=TF/SF$) in $m\,s^{-1}$. (E) One-parameter open-loop paradigm, which allows arbitrary patterns to be defined with respect to the fly's body coordinates, irrespective of its flight speed. Open-loop stimulation requires measuring the fly's position (symbolized by the two cameras) and controlling the pattern in real-time (black arrow). (F) Open-loop stimulation is required to characterize the transfer properties of the visual speed response in the two-dimensional TF–SF parameter space.

observed in tethered flying fruit flies (Fry et al., 2005). Third, turning responses have been characterized from their open-loop transfer properties (see above) whereas speed responses have been characterized from the stable-state flight conditions reached under different experimental conditions. While the latter approach can provide insights into the visual mechanisms at play when the
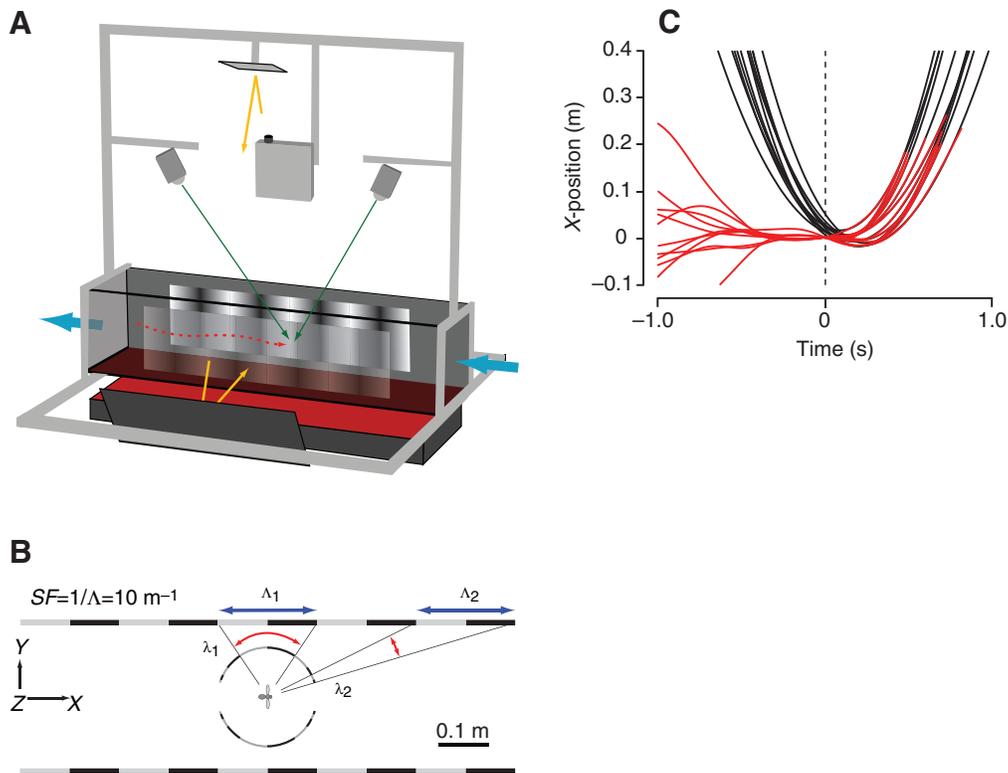
Fig. 2. Experimental setup and measurement procedure. (A) TrackFly. The free-flight experimental setup consisted of a wind tunnel (only the working section is shown) equipped with a real-time 3-D position tracking system (Trackit 3D) (Fry et al., 2000; Fry et al., 2004) and custom-programmed graphical rendering software (based on the VisionEgg) (Straw and O'Carroll, 2003; Straw et al., 2006). Flies were induced to fly upwind (red dotted arrow shows the flight direction of fly; blue arrows indicate wind direction), while their position was tracked in real time (green arrows pointing from cameras). Visual stimuli were projected onto the sidewalls *via* pairs of mirrors (yellow arrows show the light path from the projector to the screen for one side of the wind tunnel). The virtual reality features of TrackFly were used to implement a one-parameter visual open-loop paradigm [see text and Fry et al. (Fry et al., 2008) for further details]. (B) Definition of linear and angular coordinate systems. A plan view of the screens (sine gratings are represented by stripes for clarity) is shown to scale. The linear spatial frequency (SF, in m^{-1}) of the pattern displayed on the screen corresponds to the inverse of the linear spatial pattern period (Λ, in m). In the example, $SF=10\,\text{m}^{-1}$ and thus $\Lambda=0.1\,\text{m}$. The angular period (λ, unit: deg.) of the displayed patterns depends on the azimuth, with λ decreasing toward frontal and caudal positions (note red arrows). Angular spatial frequency (sf, in deg.$^{-1}$), the inverse of λ, therefore increases toward frontal and caudal positions. The linear wavelength ($\Lambda1$, $\Lambda2$) and linear spatial frequency SF remain constant. (C) Sample acceleration responses and parameter extraction. The time course of body position along the wind tunnel (red traces) is shown for 11 measurements performed under identical stimulus conditions. Flies were first held near the middle of the wind tunnel by controlling the pattern speed ($t<0$). At $t\geq0$, the flies were stimulated in open-loop ($TF=4\,\text{s}^{-1}$; $SF=12.5\,\text{m}^{-1}$; stimulus condition is marked with an asterisk in Fig. 4A). Flies reacted to the back-to-front image motion by accelerating forward, as indicated by the exponential increase of the position function (red traces, right part of the plot). Mean acceleration of each sample was measured from the fitting parameters of a parabola ($t>0.1\,\text{s}$, black traces). These values were then averaged over the trials to obtain the response strength for a single TF–SF combination (each marked with a dot in Fig. 3 and Fig. 4). Figure modified from Fry et al. (Fry et al., 2008).

insect flies at its preferred flight speed, e.g. from the observed invariance to pattern spatial frequency and contrast, it is unsuited to explore how flight speed is actually controlled from varying optic flow conditions. For this, transient responses need to be measured in the presence of experimentally defined optic flow stimuli that vary over a large spatio–temporal parameter range.

'One-parameter open-loop' free-flight paradigm
To this end, we implemented a novel behavioral paradigm that allowed us to measure visual speed responses under free-flight conditions, while controlling pattern motion in open-loop (Fig. 1E) using 'TrackFly' (Fig. 2) (Fry et al., 2008). To do so, we equipped a wind tunnel with a real-time 3-D path tracking system, i.e. Trackit 3D (Biobserve GmbH, Bonn, Germany) (see also Fry et al., 2004) and an image rendering system, i.e. the VisionEgg (v. 1.0; www.visonegg.org) (Straw et al., 2006). By experimentally de-coupling the retinal slip from the fly's flight speed, we were able to measure the open-loop transfer function over a broad range of

spatio–temporal frequencies (Fig. 1F). Automation from software control allowed us to collect a large data set of visual responses ($n=12,711$ trials) to a broad range of visual stimulus parameters.

Our results show that visual control of flight speed in fruit flies depends on linear pattern velocity ($V=TF/SF$) over a broad range of spatio–temporal frequencies (for definitions of V, TF and SF, see Coordinate system in Materials and methods). Furthermore, visual responses are largely invariant to spatial frequency composition, image contrast and wind speed. Our results suggest the presence of a sophisticated motion-processing pathway that is able to robustly extract V as a control signal for flight speed control.

MATERIALS AND METHODS
Animals
Fruit flies (*Drosophila melanogaster* Meigen) were obtained from a stock descended from a wild-caught population of 200 mated females. A standard breeding procedure was adopted, in which flies were bred from 25 females and 10 males and reared on standard

nutritive medium on a 12h:12h light:dark cycle. 2–4-day-old male and female flies were isolated and deprived of food, but not water, for 12–16h preceding an experiment. Experiments were performed during the first 6h of the subjective day.

TrackFly experimental setup

Experiments were performed using TrackFly; a wind tunnel equipped with virtual reality display technology, described in more detail elsewhere (Fry et al., 2008). In the present study, we provide an overview of the system components that are principally relevant for the understanding of the concepts and methodology applied in the present study.

Wind tunnel

The behavioral tests were performed in a commercial, open-circuit, closed-throat wind tunnel (Engineering Laboratory Design, Inc., Lake City, MN, USA). The wind tunnel provided a laminar airflow in a working section made of clear acrylic, 1.55m in length and ≤0.305m in width and height. Standard tests were performed using a wind speed of 0.29m s^{-1}. To motivate the flies to fly upwind, we vaporized an attractant odor ('Kressi' herb vinegar, diluted to 5% water solution) using an ultrasonic humidifier (Boneco, Plaston AG, Widnau, Switzerland) at a rate of ~7.2mg s^{-1} from four nozzles positioned in front of the air intake end of the wind tunnel. This procedure provided a homogenous dispersal of the odor, thus preventing a plume structure or a concentration gradient that the flies could have used as additional cues.

Real-time position tracking

Flies were tracked from above using Trackit 3D (Fry et al., 2004), equipped with two infrared-sensitive video cameras. Homogeneous back lighting was provided from a custom-built lamp emitting in the long wavelength spectrum (>700nm). Fruit flies are comparatively insensitive to long wavelengths (Heisenberg and Buchner, 1977; Stark and Johnson, 1980) and, consistently, we did not notice any effects resulting from the light shining from below. The three-dimensional (3-D) position of single flies was transferred with short delay to a client computer at a rate of 50Hz using a TCP/IP (Transmission Control Protocol/Internet Protocol) network interface.

Image rendering and display

On the client computer, visual stimuli were rendered using custom programmed software based on the VisionEgg open-source image rendering library (Straw and O'Carroll, 2003; Straw et al., 2006). The images were displayed at a refresh rate of 60Hz on a flicker-free LCD (liquid crystal display) projector (Sony, VPL-ES1, Tokyo, Japan). The image was split and projected *via* mirrors onto tracing paper screens (1.0m×0.3m) attached to the sidewalls of the wind tunnel (Fig. 2A). Various calibrations and control measurements were performed to ensure that the patterns defined in the software were displayed faithfully onto the wind tunnel screens. The average latency of TrackFly between measuring the fly's position and displaying the position-dependent stimulus was 0.038s.

Coordinate system

Throughout the text, capitalized and non-capitalized symbols are used to denote linear and angular metrics, respectively. We define the spatial frequency [*SF* (unit: m^{-1})] of the displayed sine grating, with reference to the sidewalls of the wind tunnel, as the number of cycles per unit length of the visual display (Fig. 2). Accordingly, linear pattern wavelength (Λ) is given by $\Lambda=1/SF$ (unit: m). $+X$

denotes upwind direction. The temporal frequency (*TF*) of the pattern is defined as the number of cycles passing a given point of the display per unit time (unit: s^{-1}) positive upwind. In the present experiments, *TF* and *SF* were varied systematically.

Due to perspective distortion of the pattern as viewed by the fly, the angular spatial frequency (*sf*) and angular velocity (*v*) are not constant across the visual field but instead vary with azimuth. Alternatively, we could have stimulated the flies with a single *sf* by rendering a cylindrical projection of the pattern centered on the fly (Fry et al., 2008). Such experiments are indeed useful to test specific hypotheses about optic flow processing (N.R. and S.N.F., in preparation); however, this was not the aim of the present study. To instead explore how the fly controls its flight speed with respect to realistic optic flow conditions, we displayed planar patterns; these appear largest and fastest in the lateral field of view, just like any object a fly passes by under natural free-flight conditions (e.g. David, 1982; Srinivasan et al., 1996).

Measurement procedure
Process automation

The detailed measurement of a response surface over a broad *TF*–*SF* parameter space required a large number of trials. We automated the measurement procedure by implementing the 'optomotor clamp' procedure inspired by David's (David, 1982) earlier approach. For this, we manipulated the perceived visual flight speed of the flies by varying the horizontal speed of a sine grating pattern (*SF*=6.66m^{-1}), depending on the fly's position in the wind tunnel. If the fly was too far upwind, we simulated fast, forward flight by increasing the downwind pattern speed, in response to which the fly reduced flight speed and drifted downwind. Likewise, if the fly was too far downwind, we simulated slow, forward flight by decreasing the downwind pattern speed, in response to which the fly increased flight speed and moved upwind. In consequence, the fly was kept hovering near the middle of the wind tunnel (*X*=0), where the pattern was moving at the flies' preferred speed. A test was performed as soon as a fly was measured to hover stably near the center of the wind tunnel.

'One-parameter open-loop' testing paradigm

Individual flies were stimulated for 1s with a moving sine grating, defined by *TF* and *SF*. To hold *TF* constant with respect to the fly (open-loop condition), the pattern phase was continually adjusted according to the fly's current position along the wind tunnel. Thus, only one parameter, the *TF* of the horizontal optic flow stimulus, was controlled in open-loop, i.e. decoupled from the fly's resulting behavioral response. All other sensory feedback, such as mechanosensory feedback from the halteres or antennae, remained under natural closed-loop conditions. This measurement paradigm is accurately termed 'one-parameter open-loop' condition but for simplicity we will use the term 'open-loop condition' throughout the paper. The fly's 3-D positions were logged, together with the stimulus conditions, to a data file for later analysis.

The testing protocol consisted of four test conditions and a control condition (*TF*=–2Hz, *SF*=10m^{-1}), which were repeated sequentially until sufficient data were acquired for each pattern condition. We used the control condition to detect any significant differences in response strength that might have resulted from inter-individual differences or uncontrolled experimental conditions; however, this never occurred and the variability of the responses was consistently low (Fig. 4C). We therefore pooled the data and treated them as independent. Our approach was further justified by the large number of trials performed
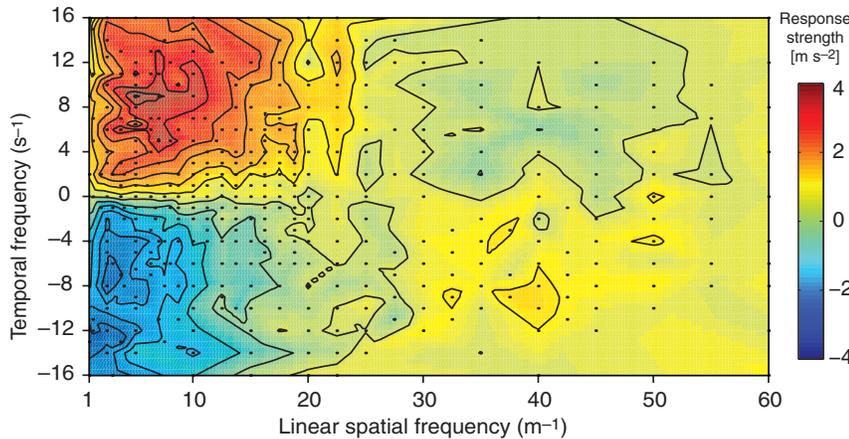
Fig. 3. Spatio–temporal tuning of speed responses. Body acceleration is shown color coded as a function of the open-loop temporal frequency (*TF*) and linear spatial frequency (*SF*) of presented sine grating stimuli. Contour lines show iso-response curves at intervals of $0.5\,\mathrm{m\,s^{-2}}$. The response surface was obtained by linearly interpolating over 435 parameter conditions, each indicated by a dot. These were calculated from a total of 12,711 trials.

(e.g. *n*=12,711 for Fig. 3). Although the exact number of flies tested is unknown, we estimated it to be in the order of *N*=1000, based on our observation that a single fly contributed about 10 trials on average.

Tests with a photographic image

We also tested the flies' responses to a moving photographic image containing a naturalistic mixture of spatial frequencies. The image is one of a set in which each image evoked similar responses of LPTCs in the hoverfly [image D in Straw et al. (Straw et al., 2008); see Movie 1 in supplementary material]. In this case, the pattern velocity was controlled in open-loop as to maintain a constant $V = TF/SF$ with respect to the fly.

Data analysis

The flies responded to open-loop regressive (back-to-front) motion stimuli with a constant forward acceleration (Fig. 2C) that depended on stimulus conditions. A constant acceleration is consistent with a constant net forward thrust, suggesting that the aerodynamic effects of varying air speed on the wings and the body are compensated. This view is consistent with the previously mentioned invariance of flies to wind speed (see Introduction).

We extracted the acceleration from the raw *X*-position data as a measure of response strength by fitting a second-order polynomial (Fig. 2C) of the form:

$$p_X(t) = p_1 t^2 + p_2 t + p_3, \qquad (1)$$

where p_X represents the fly's position along the wind tunnel (p_1, p_2 and p_3 are the fitting coefficients and *t* is the time). The mean acceleration during the trial was then determined from the second derivative:

$$\ddot{p}_X = 2p_1. \qquad (2)$$

The fitting procedure allowed the mean acceleration to be robustly measured even if the flies remained within the tracking range of the cameras for less than the entire 1 s stimulation period. Occasional outliers (fewer than 2%, typically resulting due to the presence of a second fly) were identified from an R^2 value below 0.9 and removed from the analysis. At least 10 successful trials for each condition were averaged to obtain a measurement for a particular *TF*–*SF* combination used for the subsequent analysis.

Response surface in *TF*–*SF* parameter space

Because the spatio–temporal properties of a moving sine grating are uniquely described by its *TF* and *SF*, the measured responses are appropriately represented in a two-dimensional parameter space using *TF* and *SF* as Cartesian coordinates (Fig. 3). We interpolated the accelerations measured from 435 different pattern conditions (*n*=12,711 trials) using Matlab's (The MathWorks Inc., Natick, MA, USA) griddata function (linear method). The accelerations are represented in color code, with 'hot' and 'cold' colors representing up- and downwind accelerations, respectively (Fig. 3; see Fig. 2B for sign conventions).

RESULTS

Open-loop response transfer function

Applying an automated one-parameter open-loop paradigm, we characterized the flight speed response from its behavioral open-loop transfer function, measured from 435 different pattern combinations and a total of 12,711 individual trials. Maximal upwind accelerations (upper left of Fig. 3) are observed for *TF* around $8\,\mathrm{s^{-1}}$ and *SF* around $5\,\mathrm{m^{-1}}$. At $SF \approx 25\,\mathrm{m^{-1}}$, we observe a response inversion, which is consistent with spatial aliasing at the spatial resolution limit of the fly's eye. The response structure of downwind accelerations (lower left of Fig. 3) is similar, albeit less clear and shifted toward lower *SF*s.

Superficially, the measured speed response tuning is reminiscent of that computed from a basic correlation-type motion detector (compare upper half of Fig. 3 with Fig. 1B) for rotating patterns. First, the measured speed responses show a response plateau in a limited range of *TF* and *SF* similar to the response maximum predicted by the correlator model due to its spatio–temporal band-pass filter properties (Fig. 1B). Second, the speed responses diminish above $SF \approx 25\,\mathrm{m^{-1}}$ and reverse direction (note blue color code indicating backward accelerations for *SF* around $30–55\,\mathrm{m^{-1}}$), as predicted by the correlation model.

It would be premature, however, to postulate a basic correlation-type motion detection process from these observations, which are well explained by constraints of the visuomotor system rather than a common process of motion computation. The measured response plateau, on the one hand, results from a locomotor limit in flight speed attainable in the wind tunnel, as described in detail below. The response attenuation and inversion, on the other hand, is explained with spatial aliasing and a reduction of the contrast above the Nyquist spatial frequency or twice the inter-ommatidial angle [$2\Delta\Phi$=9.6 deg., see fig. 3 in Götz (Götz, 1965)]. The maximal value of angular wavelength (λ_{max}) perceived in the fly's lateral field of view (in deg.) is calculated from:

$$\lambda_{max} = a\tan\left(\frac{1}{2SFd}\right) \times 2 \times 180/\pi, \qquad (3)$$
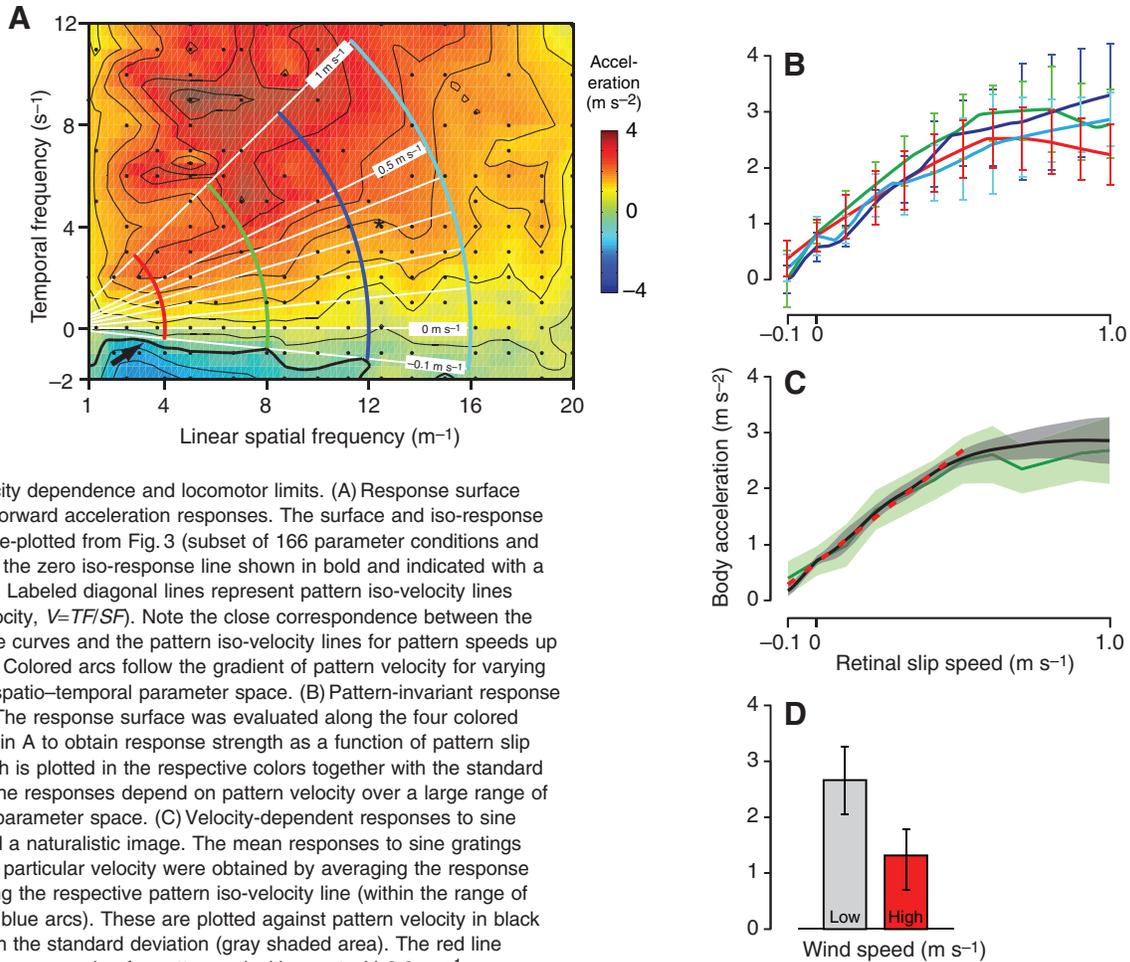
Fig. 4. Velocity dependence and locomotor limits. (A) Response surface relevant to forward acceleration responses. The surface and iso-response curves are re-plotted from Fig. 3 (subset of 166 parameter conditions and 6245 trials); the zero iso-response line shown in bold and indicated with a black arrow. Labeled diagonal lines represent pattern iso-velocity lines (pattern velocity, *V*=*TF*/*SF*). Note the close correspondence between the iso-response curves and the pattern iso-velocity lines for pattern speeds up to 0.5 m s^{-1}. Colored arcs follow the gradient of pattern velocity for varying radii in the spatio–temporal parameter space. (B) Pattern-invariant response properties. The response surface was evaluated along the four colored arcs shown in A to obtain response strength as a function of pattern slip speed, which is plotted in the respective colors together with the standard deviation. The responses depend on pattern velocity over a large range of the *TF*–*SF* parameter space. (C) Velocity-dependent responses to sine gratings and a naturalistic image. The mean responses to sine gratings moving at a particular velocity were obtained by averaging the response surface along the respective pattern iso-velocity line (within the range of the red and blue arcs). These are plotted against pattern velocity in black together with the standard deviation (gray shaded area). The red line shows a linear regression for pattern velocities up to *V*<0.6 m s^{-1} (R^2=0.985; see text for further details). Mean responses to a photographic image moving at various velocities are plotted in green together with the standard deviation (shaded). (D) Air speed saturation. Median and 25 percentile values of maximal forward accelerations induced with strong motion stimuli (*V*⩾0.6 m s^{-1}; *SF*<25 m^{-1}) in presence of low (left: −0.29 m s^{-1}; *N*=941) and high (right: −0.73 m s^{-1}; *N*=45) wind speeds. The measured accelerations reveal a significant dependence on the wind speed, suggesting an air-speed-dependent response saturation (Wilcoxon test, *P*<0.001).

with *d*=0.15 m the lateral distance of the fly from the pattern. Using *SF*=25 m^{-1} as the approximate *SF* at which the response inversion occurs, we calculate $\lambda_{max}\approx15.2$ deg. Because λ decreases toward frontal and caudal azimuths, λ will be close to or below the spatial resolution limit of the eye in most parts of the visual field. Although not directly comparable due to the different geometries of the experimental setups, it appears likely that the response inversion observed in our experiments results from spatial aliasing.

In conclusion, the conspicuous similarities between the measured response surface and the tuning properties of a basic correlation detector circuit reflect physiological constraints of the visuomotor system rather than a common motion processing mechanism.

A further constraint explains the previously mentioned differences in upwind- and downwind-directed speed responses (positive and negative accelerations in Fig. 3, respectively). When accelerating upwind, the flies kept their body orientation closely aligned with the wind tunnel long axis, as confirmed with high-speed recordings made from the side through a slit in one of the display screens (see Movie 1 in supplementary material). There must be limits, however,

to the degree with which the flies compensate increasing tailwinds with deceleration, as this would eventually lead to the somewhat paradoxical situation of flies flying backward with respect to the surrounding air. Indeed, the flies tolerated only little front-to-back retinal slip before they reversed their body orientation, as revealed by high-speed video analysis (data not shown). Likewise, Kennedy (Kennedy, 1939) identified a threshold for front-to-back pattern motion, above which mosquitoes reversed their flight direction and flew downwind. Because the retinal stimulation changed along with the fly's turning responses, the data are difficult to interpret and were therefore excluded from further analysis.

Visual encoding properties of the speed response
To gain insight into the strategy of visual control of flight speed, we focused our analysis on forward-directed acceleration responses in a reduced parameter range that is most likely to be relevant for flight speed control (Fig. 4A). Because previous research has shown that preferred flight speed depends on pattern velocity (see Introduction), it is meaningful to evaluate the response surface in

view of identical pattern velocities represented by the different combinations of TF and SF. The linear velocity V of a sine grating corresponds to the ratio of its TF and SF ($V=TF/SF$). Therefore, all sine gratings that move at a particular V fall onto a diagonal line through the origin with slope $V=TF/SF$. For example, the $0.5\,\mathrm{m\,s^{-1}}$ pattern iso-velocity line connects all TF and SF coordinates for which $V=TF/SF=0.5\,\mathrm{m\,s^{-1}}$, such as (6,12) and (2,4).

Pattern iso-velocity lines for $-0.1{\leq}V{\leq}1\,\mathrm{m\,s^{-1}}$ are shown as labeled white lines superimposed over the response surface shown in Fig. 4A. Whereas the Cartesian TF–SF coordinate system describes the patterns from their temporal and spatial frequency composition, the superimposed polar coordinate system describes the patterns in terms of their velocity, with the angular coordinate $\alpha=\tan(V)$. The radial coordinate $r=\sqrt{(TF^2+SF^2)}$ describes whether a moving sine grating is composed of high or low spatio–temporal frequencies. As shown below, the measured response characteristics are suitably evaluated with respect to their velocity characteristics (i.e. the polar coordinates), rather than their spatio–temporal tuning properties (the Cartesian coordinates).

Set-point transfer properties

We first evaluate the measured response surface in view of the previous finding that the 'preferred' flight speed of free-flying insects is invariant to the spatial pattern properties (see Introduction). In control terms, the 'preferred' flight speed represents the controller's set point, which defines the stable equilibrium under normal closed-loop conditions. In an open-loop input–output function, the set point is identified from a zero crossing of a response function, with a positive slope indicating a stable equilibrium point (Strogatz, 1994). If consistent with previous free-flight data, we would expect our response surface to reveal a zero response contour line (the zero-crossing) that is flanked by a positive response gradient (required for closed-loop stability) and follows a pattern iso-velocity line (required for pattern invariance).

As shown in the lower part of Fig. 4A, the zero response contour line (shown bold and marked with a black arrow) indeed runs roughly diagonally, corresponding to a pattern velocity of approximately $-0.15\,\mathrm{m\,s^{-1}}$ (i.e. front-to-back). This preferred pattern velocity is similar to the preferred flight speed of $D.\ melanogaster$ measured in free flight (Tammero and Dickinson, 2002). Our data show that the preferred pattern velocity of $D.\ melanogaster$ spans a roughly 8-fold range of SF (between about 2–$16\,\mathrm{m^{-1}}$), consistent with previous findings in honeybees (Baird et al., 2005).

The findings based on the zero response iso-line measured under open-loop conditions are consistent with previous data measured under closed-loop flight conditions, validating our experimental approach for a functional analysis of free-flight control.

Pattern velocity as a control signal for corrective speed maneuvers

The particular shape of the response surface reveals the spatio–temporal pattern properties relevant for speed control and how corrective speed maneuvers depend on them. Over a broad range of the response surface shown in Fig. 4A, the response iso-lines are roughly aligned with the diagonally oriented pattern iso-velocity lines, suggesting a close correspondence between the response strength and pattern velocity, rather than a response tuning to a particular combination of TF and SF.

To quantify the dependence of response strength on the open-loop pattern velocity, or retinal slip speed (V_{slip}), we evaluated the response surface along four radial paths in the two-dimensional TF–SF parameter space (red, green, dark blue and light blue arcs in Fig. 4A, with r values of 4, 8, 12 and 16, respectively). The responses, sampled over a broad TF–SF parameter space, show a similar dependence on V_{slip} and are statistically indistinguishable from one another. The responses increase with V_{slip} and saturate at around $3\,\mathrm{m\,s^{-2}}$ for $V_{\mathrm{slip}}>0.6\,\mathrm{m\,s^{-1}}$ (Fig. 4B). The variance of the mean responses (likewise linearly interpolated) is shown with error bars for the 48 measurement conditions. The standard deviation is roughly constant at about $\pm0.5\,\mathrm{m\,s^{-2}}$ and increases to about twice this value at high retinal slip speeds.

Averaging the responses measured for radii between 8 and 16 (i.e. along the pattern iso-velocity lines between the red and light blue arcs in Fig. 4A) reveals a linear-dependence ($R^2=0.985$) of response strength for $V_{\mathrm{slip}}<0.6\,\mathrm{m\,s^{-1}}$, above which the responses saturate at around $3\,\mathrm{m\,s^{-2}}$ (black line in Fig. 4C). Within the linear range, therefore, the flies' accelerations depend directly on the linear pattern velocity $V=TF/SF$ as the relevant visual control parameter for flight speed.

Linearity in response provides constant reaction time

The linearity of the response function within the dynamic range is a remarkable characteristic of the visual control of flight speed, the functional relevance of which, however, remains unknown. In control theory terms, the measured slope of $3.73\pm0.11\,\mathrm{s^{-1}}$ corresponds to the open-loop gain (G_{OL}) of a purely proportional control system. The zero crossing of the acceleration at $-0.17\,\mathrm{m\,s^{-1}}$ preferred flight speed corresponds to the controller's set point velocity (V_{set}). The linear regression of the measured acceleration (Acc) is:

$$Acc = G_{\mathrm{OL}}\,(V_{\mathrm{slip}} - V_{\mathrm{set}})\,, \qquad (4)$$

with a R^2 value of 0.985. Under the simplifying assumption that the fly's acceleration response remains constant throughout the short response duration (but see below), the time required for the fly to attain V_{set} after a visual perturbation is calculated from:

$$\mathrm{T} = (V_{\mathrm{slip}} - V_{\mathrm{set}})\,/\,Acc\,. \qquad (5)$$

Combining Eqn 4 and Eqn 5 shows that the reaction time (T) is the inverse of the G_{OL} and is therefore constant under the given assumptions:

$$\mathrm{T} = 1\,/\,G_{\mathrm{OL}}\,. \qquad (6)$$

Using the measured value of G_{OL}, we estimated the duration of the acceleration response at $0.27\,\mathrm{s}$. This value represents a lower estimate because, in reality, the fly's acceleration decreases with the velocity error signal (V_{slip}–V_{set}) as the fly's speed approaches V_{set}.

T relates only to the period of constant acceleration and does not include a constant response time lag of approximately $0.10\,\mathrm{s}$ (see Fig. 2C, analysis not shown). We therefore estimate the total time required by the fly to correct a visual perturbation to lie slightly above $0.37\,\mathrm{s}$. A more detailed analysis of the control properties will be presented elsewhere (N.R. and S.N.F., in preparation).

Speed responses are robust for SF composition and image contrast

Previous research has explored the possibility that pattern invariance could arise in a correlation-based motion-processing pathway from the processing of images with a broad spatial frequency spectrum, as is found in natural visual environments of flies (see Introduction). Indeed, stimulation with a broad SF spectrum is expected to result in more meaningful responses if non-linearities in the visual system operated on various spatial frequency components. To test this

possibility, we measured flight speed responses in the presence of a moving photographic image that was used in a previous electrophysiological study to reflect the broad spatial frequency spectrum of a fly's natural habitat (Straw et al., 2008). We controlled the image velocity in open-loop and measured the resulting acceleration responses as before. Whereas the previous experiments used a single *TF–SF* combination for individual trials, the image presentation experiments tested the responses to a simultaneous presentation of *TF–SF* combinations, corresponding to numerous points along the respective iso-velocity line in the *TF–SF* parameter space.

The responses to the photographic image were indistinguishable from the averaged responses measured using sine gratings (compare green and black traces in Fig. 4C). We therefore conclude that the computation of pattern velocity by the fly's visual system is largely invariant for spatial frequency content of the planar patterns. Single *SF*s and a broadband photographic image both lead to robust flight velocity control.

Additionally, although image contrast differed considerably between the sine grating (Michelson contrast: C=0.5) and the photographic image [see image C in Straw et al. (Straw et al., 2008); see also for a discussion of contrast metrics for natural images], this did not lead to a significant difference in response strength, suggesting that speed responses are largely contrast invariant, consistent with recent findings in honeybees in a similar behavioral context (Baird et al., 2005). A biologically plausible explanation for contrast invariance could lie in contrast saturation in the early visual system (Dror et al., 2001), although other mechanisms are known to be responsible for contrast insensitivity observed in the tangential cells of other fly species (Straw et al., 2008).

Response saturation

As shown above, accelerations reached a plateau of about $3\,\text{m}\,\text{s}^{-2}$ at pattern speeds above $0.6\,\text{m}\,\text{s}^{-1}$. The underlying cause of the response saturation is relevant to the understanding of the underlying control mechanisms. We consider two likely explanations for the saturation. First, saturation could occur in the visual pathways, limiting the encoding of pattern speeds to a particular value. Second, the saturation could result from locomotor limits, either due to an upper limit in acceleration of $3\,\text{m}\,\text{s}^{-2}$ or in the maximum air speed attainable by the fly due to increasing drag acting on the wings and body [for drag effects on the wing, see also Hesselberg and Lehmann (Hesselberg and Lehmann, 2007)].

To distinguish between these two possibilities, we compared the accelerations reached under standard wind conditions ($-0.290\,\text{m}\,\text{s}^{-1}$) with those measured in the presence of an increased headwind ($-0.73\,\text{m}\,\text{s}^{-1}$) (Fig. 4D). Increasing the headwind caused a significant reduction of the acceleration from 2.67 to $1.32\,\text{m}\,\text{s}^{-2}$ (Fig. 4D), indicating that the response saturation did not result from a limit of pattern velocities extracted by the visual system but instead depended on the air speed. Apparently, the flies reached an upper limit of air speeds at which they were able or willing to fly. When flying below their maximum air speed, the flies' acceleration was invariant to the wind speeds tested (data not shown), in accordance with results published for various insect species [e.g. Aedes (Kennedy, 1939); Aphis (Kennedy and Thomas, 1974); *D. virilis* (David, 1982); Apis (Barron and Srinivasan, 2006)].

DISCUSSION
Open-loop stimulation and response tuning

To gain a functional understanding of optic flow processing for flight speed control, we applied a one-parameter open-loop paradigm in free-flying fruit flies. A single fly at a time was induced to hover near the center of the wind tunnel, where we briefly stimulated it with a moving sine grating. During the 1 s stimulation, we compensated for changes in the fly's position by adjusting the phase of the displayed pattern in real time, such that the temporal frequency of the pattern was held constant with respect to the fly. This experimentally induced open-loop condition allowed us to characterize the fly's visual flight speed response using retinal temporal frequency and spatial frequency as independent control parameters (Fig. 3; Fig. 4A).

While our method allowed us to characterize an important free-flight reflex in a two-dimensional spatio–temporal parameter space, the one-parameter open-loop condition was experimentally induced, raising the question of whether our measurements were subject to artefacts, resulting from the highly artificial experimental conditions.

A first question relates to other sensory modalities, such as mechanosensory feedback from the halteres and antennae and olfactory cues, which remained in closed-loop and might have provided conflicting cues. The experimentally induced disparity between the visual and other sensory inputs is in fact by no means unnatural and mimics a control scenario faced by a fly flying upwind quite closely. Whether flying against a constant wind or in still air, a fly adjusts its air speed so as to maintain a constant 'preferred' retinal pattern slip speed [see fig. 3 in David (David, 1982)] (see also Introduction). This situation is similar to our pre-test condition, in which the fly was induced to hover near the middle of the wind tunnel, where the visual pattern motion matched the fly's preferred retinal slip speed. In a natural environment, a gust of wind from the front could easily cause the fly to momentarily slow down or even be carried backward, in which case the fly would perceive regressive (back-to-front) retinal slip. At this moment, the retinal slip depends largely on the strength of the wind gust and not the fly's behavior; a situation closely corresponding to the open-loop condition we implemented using TrackFly.

While mechanosensory input is likely to provide information about the fly's air speed [e.g. from the antennae (Gewecke, 1967; Taylor and Krapp, 2008)], there is no mechanism besides vision known to provide the fly with a reference for its ground speed. In this context, it is interesting to consider the role of the halteres, which sense the Coriolis forces associated with angular body velocity but probably not the much weaker forces resulting from linear accelerations (Pringle, 1948; Nalbach, 1993; Nalbach and Hengstenberg, 1994). The halteres are therefore part of an inner control loop mediating changes in body pitch, as required for flight speed control (David, 1978; Dickson et al., 2008), but are unlikely to affect the outer control loop, which appears to be driven by pattern velocity alone (Fig. 5). Our one-parameter open-loop paradigm therefore selectively provided experimental access to the outer, visually mediated control loop, while other sensory modalities remained under realistic closed-loop conditions, as required for realistic free-flight control.

A second question relates to the de-coupling of retinal slip speed from the fly's behavior, which to be perfect would require controlling the stimulus with zero time delay. Instead, the total system latency of TrackFly was $\tau=38\,\text{ms}$ (see Materials and methods), which is in the order of the fastest visual behaviors documented in free-flying flies [e.g. 30 ms in chasing *Fannia* (Land and Collett, 1974)]. The difference between the intended and the actual stimulation was previously calculated for the present testing paradigm, assuming a constant $\tau=38\,\text{ms}$ and that the flies responded with a constant acceleration (Fig. 2B). After 20 ms, the actual slip speed reached a constant level that was reduced by 7.6% compared with the desired slip speed [see fig. 6 in Fry et al. (Fry et al., 2008)]. Correcting our
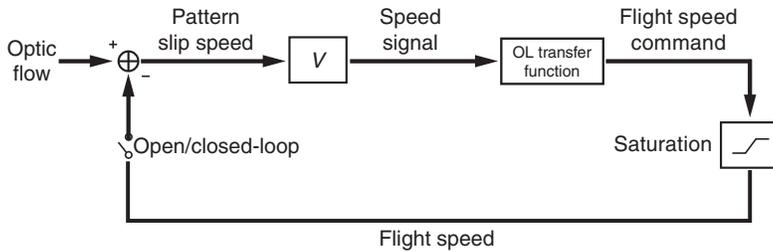

parameter space. Such comparisons may be possible due to recent advances in electrophysiological techniques, which have allowed recording from LPTC in *Drosophila* (Joesch et al., 2008).

Furthermore, the measurement of the transient response properties to a step change in sensory input will allow a more detailed evaluation of the underlying motion computations. It is essential to assess whether transient or steady-state response properties of the motion-processing pathways dominate at the behaviorally relevant time scales (Borst and Bahde, 1986). Recent electrophysiological studies in flies have explored transient response properties of motion pathways in playback experiments that used realistic optic flow stimuli reconstructed from free-flight behavior (e.g. Kern et al., 2005; Karmeier et al., 2006). The finding that the steady-state physiology of a visual interneuron does not predict its response to more dynamic stimuli emphasizes the importance of re-examining behavioral responses under transient conditions, as performed in our present study.

Outlook

Future studies combining advanced genetic techniques with detailed behavioral analyses promise advances in our understanding of the neural substrate for motion processing in different behavioral contexts. For example, identified motion processing neurons can be genetically targeted (Joesch et al., 2008), which will allow them to be manipulated to explore their involvement and possible role from the behavioral effects (Duffy, 2002). In a recent study, a forward genetic approach was applied in walking *Drosophila* and selective effects of large field optic flow were identified on walking speed and turning responses. Based on these results, it has been proposed that visual pathways subserving the control of translation and rotation may separate at the earliest stage of visual processing (Katsov and Clandinin, 2008). It will be highly informative to combine advanced genetic techniques with detailed flight control analyses in a meaningful functional context to explore the physiological basis of speed control. In particular, genetic modification of the known visual pathways may provide evidence for the involvement and role of the known pathways in the context of visual control of flight speed.

Finally, our results are of direct relevance for biomimetic robotic implementations, such as autonomous flying micro-robots. We showed that visual speed control is based on a remarkably simple control strategy, however, requires a sophisticated vision sensor to robustly signal the linear pattern speed. Our work suggests that the fly's speed control strategy could be meaningfully transferred into the context of autonomous micro air vehicles, while substituting the complex biological control mechanisms with functionally equivalent engineering solutions.

LIST OF ABBREVIATIONS

Acc	acceleration
EMD	elementary motion detector
G_{OL}	open-loop gain
LPTC	lobula plate tangential cells
r	radius in *TF–SF* parameter space
SF	linear spatial frequency
sf	angular spatial frequency
sf_{opt}	optimal angular spatial frequency for correlator
T	reaction time
TF, tf	temporal frequency
tf_{opt}	optimal temporal frequency for correlator
V	linear pattern velocity
v	angular pattern velocity
V_{pref}	preferred pattern velocity
V_{slip}	retinal pattern slip speed
V_{set}	set point pattern velocity
X, p_X	fly's upwind position in the wind tunnel
α	angular coordinate in *TF-SF* parameter space
λ	angular pattern wavelength
Λ	linear pattern wavelength
ΔΦ	inter-ommatidial angle
τ	time delay of tracking system

REFERENCES

Baird, E., Srinivasan, M. V., Zhang, S. and Cowling, A. (2005). Visual control of flight speed in honeybees. *J. Exp. Biol.* **208**, 3895-3905.

Barron, A. and Srinivasan, M. V. (2006). Visual regulation of ground speed and headwind compensation in freely flying honey bees (*Apis mellifera* L.). *J. Exp. Biol.* **209**, 978-984.

Borst, A. and Bahde, S. (1986). What kind of movement detector is triggering the landing response of the housefly? *Biol. Cybern.* **55**, 59-69.

Borst, A. and Egelhaaf, M. (1989). Principles of visual motion detection. *Trends Neurosci.* **12**, 297-306.

Borst, A. and Haag, J. (2002). Neural networks in the cockpit of the fly. *J. Comp. Physiol. A* **188**, 419-437.

Buchner, E. (1976). Elementary movement detectors in an insect visual system. *Biol. Cybern.* **24**, 85-101.

Buchner, E. (1984). Behavioral analysis of spatial vision in insects. In *Photoreception and Vision in Invertebrates* (ed. M. A. Ali), pp. 561-621. New York: Plenum Press.

Collett, T., Nalbach, H. O. and Wagner, H. (1993). Visual stabilization in arthropods. *Rev. Oculomot. Res.* **5**, 239-263.

David, C. T. (1978). The relationship between body angle and flight speed in free-flying *Drosophila. Physiol. Entomol.* **3**, 191-195.

David, C. T. (1982). Compensation for height in the control of groundspeed by *Drosophila* in a new, 'barber's pole' wind tunnel. *J. Comp. Physiol. A* **147**, 485-493.

Dickson, W. B., Straw, A. D. and Dickinson, M. H. (2008). Integrative model of Drosophila flight. *AIAA Stud. J.* **46**, 2150-2164.

Dror, R. O., O'Carroll, D. C. and Laughlin, S. B. (2001). Accuracy of velocity estimation by Reichardt correlators. *J. Opt. Soc. Am.* **18**, 241-252.

Dudley, R. (2000). *The Biomechanics of Insect Flight: Form, Function, Evolution.* Princeton, NJ: Princeton University Press.

Duffy, J. B. (2002). GAL4 system in *Drosophila*: a fly geneticist's Swiss army knife. *Genesis* **34**, 1-15.

Eckert, H. (1973). Optomotorische Untersuchungen am visuellen System der Stubenfliege *Musca domestica* L. *Biol. Cybern.* **14**, 1.

Egelhaaf, M. and Borst, A. (1993). Movement detection in arthropods. In *Visual Motion and its Role in the Stabilization of Gaze* (ed. J. Wallman and F. A. Miles), pp. 53-77. Amsterdam: Elsevier.

Egelhaaf, M. and Kern, R. (2002). Vision in flying insects. *Curr. Opin. Neurobiol.* **12**, 699-706.

Egelhaaf, M., Kern, R. and Warzecha, A.-K. (1998). Sensory ecology and neural coding in arthropods. *Z. Naturforsch. C* **53**, 582-592.

Egelhaaf, M., Kern, R., Krapp, H. G., Kretzberg, J., Kurtz, R. and Warzecha, A. K. (2002). Neural encoding of behaviourally relevant visual–motion information in the fly. *Trends Neurosci.* **25**, 96-102.

Fermi, G. and Reichardt, W. (1963). Optomotorische reaktionen der fliege *Musca domestica. Kybernetik* **2**, 15-28.

Franceschini, N., Ruffier, F. and Serres, J. (2007). A bio-inspired flying robot sheds light on insect piloting abilities. *Curr. Biol.* **17**, 329-335.

Fry, S. N., Bichsel, M., Müller, P. and Robert, D. (2000). Tracking of flying insects using pan-tilt cameras. *J. Neurosci. Methods* **101**, 59-67.

Fry, S. N., Sayaman, R. and Dickinson, M. H. (2003). The aerodynamics of free-flight maneuvers in *Drosophila. Science* **300**, 495-498.

Fry, S. N., Müller, P., Baumann, H. J., Straw, A. D., Bichsel, M. and Robert, D. (2004). Context-dependent stimulus presentation to freely moving animals in 3D. *J. Neurosci. Methods* **135**, 149-157.

Fry, S. N., Sayaman, R. and Dickinson, M. H. (2005). The aerodynamics of hovering flight in *Drosophila. J. Exp. Biol.* **208**, 2303-2318.

Fry, S. N., Rohrseitz, N., Straw, A. D. and Dickinson, M. H. (2008). TrackFly: virtual reality for a behavioral system analysis in free-flying fruit flies. *J. Neurosci. Methods* **171**, 110-117.

Gewecke, M. (1967). Die Wirkung von Luftströmung auf die Antennen und das Flugverhalten der blauen Schmeissfliege (*Calliphora erythrocephala*). *J. Comp. Physiol. A.* **54**, 121-164.

Gewecke, M. and Heinzel, H. G. (1980). Aerodynamic and mechanical properties of the antennae as air-current sense organs in *Locusta migratoria*.1. Static characteristics. *J. Comp. Physiol. A* **139**, 357-366.

Gibson, J. J. (1958). Visually controlled locomotion and visual orientation in animals. *Br. J. Psychol.* **49**, 182-194. Reprinted in *Ecol. Psychol.* **10**, 161-176 (1998).

Götz, K. G. (1964). Optomotorische Untersuchung des visuellen Systems einiger Augenmutanten der Fruchtfliege *Drosophila*. *Kybernetik* **2**, 77-92.

Götz, K. G. (1965). Die optischen Übertragungseigenschaften der Komplexaugen von *Drosophila*. *Kybernetik* **2**, 215-221.

Hassenstein, B. and Reichardt, W. (1956). Systemtheoretische Analyse der Zeit-, Reihenfolgen- und Vorzeichenauswertung bei der Bewegungsperzeption des Rüsselkafers *Chlorophanus. Z. Naturforsch.* **11b**, 513-524.

Hausen, K. (1993). Decoding of retinal image flow in insects. *Rev. Oculomot. Res.* **5**, 203-235.

Heisenberg, M. and Buchner, E. (1977). The rôle of retinula cell types in visual behavior of *Drosophila melanogaster. J. Comp. Physiol. A* **117**, 127-162.

Hesselberg, T. and Lehmann, F.-O. (2007). Turning behaviour depends on frictional damping in the fruit fly *Drosophila. J. Exp. Biol.* **210**, 4319-4334.

Joesch, M., Plett, J., Borst, A. and Reiff, D. F. (2008). Response properties of motion-sensitive visual interneurons in the lobula plate of *Drosophila melanogaster. Curr. Biol.* **18**, 368-374.

Karmeier, K., van Hateren, J. H., Kern, R. and Egelhaaf, M. (2006). Encoding of naturalistic optic flow by a population of blowfly motion-sensitive neurons. *J. Neurophysiol.* **96**, 1602-1614.

Katsov, A. Y. and Clandinin, T. R. (2008). Motion processing streams in Drosophila are behaviorally specialized. *Neuron* **59**, 322-335.

Kennedy, J. S. (1939). The visual responses of flying mosquitoes. *Proc. Zool. Soc. Lond. A Gen. Exp.* **109**, 221-242.

Kennedy, J. S. and Thomas, A. A. G. (1974). Behavior of some low-flying aphids in wind. *Ann. Appl. Biol.* **76**, 143-159.

Kern, R., van Hateren, J. H., Michaelis, C., Lindemann, J. P. and Egelhaaf, M. (2005). Function of a fly motion-sensitive neuron matches eye movements during free flight. *PLoS Biol.* **3**, e171.

Kunze, P. (1961). Untersuchung des Bewegungssehens fixiert fliegender Bienen. *Z. Vgl. Physiol.* **44**, 656-684.

Land, M. F. and Collett, T. S. (1974). Chasing behaviour of houseflies (*Fannia canicularis*). *J. Comp. Physiol. A* **89**, 331-357.

Lindemann, J. P., Kern, R., van Hateren, J. H., Ritter, H. and Egelhaaf, M. (2005). On the computations analyzing natural optic flow: quantitative model analysis of the blowfly motion vision pathway. *J. Neurosci.* **25**, 6435-6448.

Mronz, M. and Lehmann, F.-O. (2008). The free-flight response of Drosophila to motion of the visual environment. *J. Exp. Biol.* **211**, 2026-2045.

Nalbach, G. (1993). The halteres of the blowfly Calliphora: I. Kinematics and dynamics. *J. Comp. Physiol. A* **173**, 293-300.

Nalbach, G. and Hengstenberg, R. (1994). The halteres of the blowfly *Calliphora*: II. Three-dimensional organization of compensatory reactions to real and simulated rotations. *J. Comp. Physiol. A* **175**, 695-708.

O'Carroll, D. C., Bidwell, N. J., Laughlin, S. B. and Warrant, E. J. (1996). Insect motion detectors matched to visual ecology. *Nature* **382**, 63-66.

Pringle, J. W. S. (1948). The gyroscopic mechanism of the halteres of Diptera. *Philos. R. Soc. Lond. B Biol. Sci.* **233**, 347-384.

Reichardt, W. (1961). Autocorrelation, a principle for relative movement discrimination by the central nervous system. In *Sensory Communication* (ed. W. A. Rosenblith), pp. 303-317. New York: MIT Press.

Sherman, A. and Dickinson, M. H. (2004). Summation of visual and mechanosensory feedback in *Drosophila* flight control. *J. Exp. Biol.* **207**, 133-142.

Srinivasan, M. V. and Zhang, S. (2004). Visual motor computations in insects. *Annu. Rev. Neurosci.* **27**, 679-696.

Srinivasan, M. V., Lehrer, M., Kirchner, W. H. and Zhang, S. W. (1991). Range perception through apparent image speed in freely flying honeybees. *Vis. Neurosci.* **6**, 519-535.

Srinivasan, M. V., Zhang, S., Lehrer, M. and Collett, T. S. (1996). Honeybee navigation *en route* to the goal: visual flight control and odometry. *J. Exp. Biol.* **199**, 237-244.

Srinivasan, M. V., Poteser, M. and Kral, K. (1999). Motion detection in insect orientation and navigation. *Vis. Res.* **39**, 2749-2766.

Stark, W. S. and Johnson, M. (1980). Microspectrophotometry of *Drosophila* visual pigments: determinations of conversion efficiency in R1-6 receptors. *J. Comp. Physiol. A* **140**, 275-286.

Straw, A. D. and O'Carroll, D. C. (2003). Motion blur applied to eliminate artifacts in apparent motion displays. *J. Vis.* **3**, 782.

Straw, A. D., Warrant, E. J. and O'Carroll, D. C. (2006). A 'bright zone' in male hoverfly (*Eristalis tenax*) eyes and associated faster motion detection and increased contrast sensitivity. *J. Exp. Biol.* **209**, 4339-4354.

Straw, A. D., Rainsford, T. and O'Carroll, D. C. (2008). Contrast sensitivity of insect motion detectors to natural images. *J. Vis.* **8**, 1-9.

Strogatz, S. H. (1994). *Nonlinear Dynamics and Chaos: With Applications to Physics, Biology, Chemistry, and Engineering.* Cambridge: Perseus Books.

Tammero, L. F. and Dickinson, M. H. (2002). The influence of visual landscape on the free flight behavior of the fruit fly *Drosophila melanogaster. J. Exp. Biol.* **205**, 327-343.

Taylor, G. K. and Krapp, H. G. (2008). Sensory systems and flight stability: what do insects measure and why? *Adv. Insect Physiol.* **34**, 231-316.

Taylor, G. K., Bacic, M., Bomphrey, R. J., Carruthers, A. C., Gillies, J., Walker, S. M. and Thomas, A. L. R. (2008). New experimental approaches to the biology of flight control systems. *J. Exp. Biol.* **211**, 258-266.

Wehner, R. (1992). Arthropods. In *Animal Homing* (ed. F. Papi), pp. 45-144. New York: Chapman & Hall.

Zanker, J. M., Srinivasan, M. V. and Egelhaaf, M. (1999). Speed tuning in elementary motion detectors of the correlation type. *Biol. Cybern.* **80**, 109-116.